Acta Cryst E CRYSTALLOGRAPHIC COMMUNICATIONS

ISSN 2056-9890

Solvent-free synthesis and low-temperature crystal structure of phenoquinone (the 1:2 *p*-benzoquinone–phenol complex)

A. Timothy Royappa,[a]* Jake A. Tan[a] and Dean H. Johnston[b]

[a]Department of Chemistry, University of West Florida, 11000 University Parkway, Pensacola, FL 32514, USA, and [b]Department of Chemistry, Otterbein University, 1 South Grove Street, Westerville, OH 43081, USA. *Correspondence e-mail: royappa@uwf.edu

Received 31 March 2026
Accepted 22 May 2026

Edited by S. P. Kelley, University of Missouri-Columbia, USA

Keywords: crystal structure; cocrystal; solvent-free synthesis.

CCDC reference: 2556203

Supporting information: this article has supporting information at journals.iucr.org/e

A novel solvent-free synthesis of phenoquinone (the common name for the hydrogen-bonded 1:2 *p*-benzoquinone–phenol complex, $C_6H_4O_2{\cdot}2C_6H_6O$) is reported. This 'green' method produces X-ray quality cocrystals of phenoquinone as red needles within minutes. A newly redetermined and greatly improved low-temperature (100 K) crystal structure is reported. A time-dependent density functional theory examination of the charge-transfer excitation in phenoquinone accounts for the red color of this hydrogen-bonded complex.

1. Chemical context

One definition of a cocrystal is 'a crystal that is built up out of two or more organic compounds that are, in their pure forms, solid at ambient conditions' (Vishweshwar *et al.*, 2006). Such cocrystals are gathering increased research attention in the pharmaceutical sector because cocrystals of active pharmaceutical ingredients (APIs) may have markedly improved pharmacological and pharmacokinetic properties compared to polymorphs of the pure APIs (Yadav *et al.*, 2009; Chettri *et al.*, 2024). In addition, cocrystals are also known to improve the physicochemical properties of agrochemicals, pigments, and solid explosives (Karimi-Jafari *et al.*, 2018). Nevertheless, it is still difficult to predict *ab initio* whether two compounds will cocrystallize; therefore, it is essential to have in hand many high-quality crystal structures of cocrystals for theory development and for training of machine-learning models. As a side note, phenoquinone is responsible for the faint pink color of impure phenol due to air oxidation (to *p*-benzoquinone).

Early structural studies of a cocrystal were the X-ray crystal structure investigations (Wallwork & Harding, 1953; Harding & Wallwork, 1953) of phenoquinone, which has been known for more than a century (Pratt & Gibbs, 1913). The UV-visible spectrum and kinetics of formation of phenoquinone were reported a little later, but no structural details were elucidated (Zuev, 1956; Tronov & Sokolovich, 1956). This cocrystal was studied in much greater detail by Sakurai (1968), and the resulting structure was deposited in the Cambridge Structural Database (CSD). The room-temperature structure of phenoquinone obtained by Sakurai was of rather low quality, however. Additionally, the crystallization conditions given by Sakurai were vague, consisting of the single, uninformative sentence, 'Single crystals of phenoquinone were obtained from a mixture of acetone solutions of 1:2 mol ratio of *p*-benzoquinone and phenol.' This method did not yield

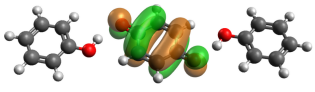
LUMO (-2.82 eV)

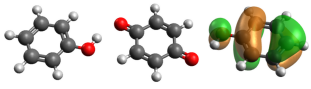
HOMO (-7.20 eV)

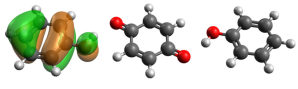
HOMO-1 (-7.22 eV)

crystals in our hands. However, we found a remarkably simple, solvent-free method that resulted in X-ray quality crystals of phenoquinone in a few minutes. Thus, the 'green' synthesis and subsequent structural characterization presented here is also of relevance to the modern method of hot-melt extrusion used to produce pharmaceutical cocrystals (Narala *et al.*, 2021) and to other green cocrystal synthesis methods, including mechanochemical synthesis (Braga *et al.*, 2013; Duarte *et al.*, 2016; Qi *et al.*, 2024).

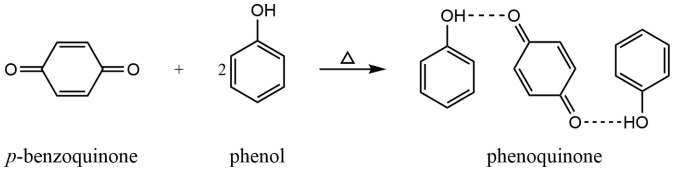

The structure described in this paper was obtained at 100 K, with multi-scan absorption correction applied and employing anisotropic displacement parameters (ADPs) for non-hydrogen atoms, resulting in much improved refinement quality compared to Sakurai's structure (R_1 = 0.0483 *vs* R_1 = 0.1050). The lower data acquisition temperature also allowed for higher precision in geometric parameters such as bond lengths and bond angles (see the *Structural commentary* section below). The difference map showed no significant residual electron density and the ADPs were small, denoting an absence of disorder in the structure.

2. Structural commentary

The general features of this crystal structure have been discussed in detail elsewhere (Wallwork & Harding, 1953; Harding & Wallwork, 1953; Sakurai, 1968). Briefly, each phenoquinone unit consists of a *p*-benzoquinone molecule on an inversion center, hydrogen bonded to two centrosymmetrically arranged flanking phenols, as shown in Fig. 1. The asymmetric unit is one-half of the phenoquinone. In this complex, the O2—H1 distance is 1.84 (2) Å [O1···O2 distance 2.732 (2) Å) and the O1—H1···O2 angle is nearly straight at 172.3 (19)°. This is an indication of much stronger hydrogen bonding than Sakurai had found (O2—H1 distance 2.05 Å, O1—H1···O2 angle 158°). Although the phenolic hydrogen H1 was placed in a riding position, an unmistakable electron density peak is observed ∼0.9 Å from phenolic oxygen O1,

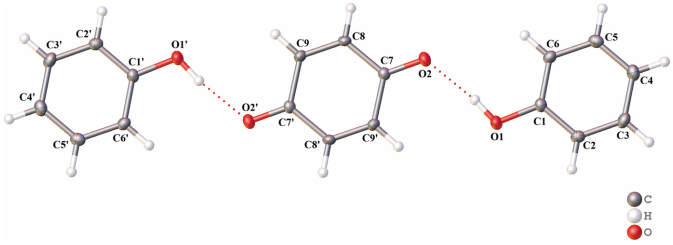

Figure 1
Hydrogen-bonded structure of phenoquinone, showing 1:2 *p*-benzoquinone:phenol stoichiometry.

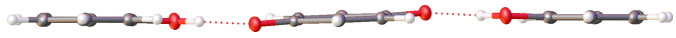

Figure 2
Side view of phenoquinone showing the planar structure of the complex.

confirming that this hydrogen atom is still clearly covalently bonded to the phenolic oxygen. The three molecules in each phenoquinone complex are coplanar, as can be seen in the side view of phenoquinone shown in Fig. 2; the r.m.s. deviation of all atoms from their mean plane is only 0.044 Å.

The phenoquinone units are stacked 3.1 Å apart in columns with their planes parallel to (301), with parallel columns forming infinite sheets. These sheets alternate with sheets of identically packed phenoquinones to generate the three-dimensional crystal structure of the solid. The angle between phenoquinone mean planes in adjacent sheets is 62.5°, as can be seen in Fig. 3, in which the structure is viewed along [001].

3. Supramolecular features

Phenol itself is colorless and *p*-benzoquinone is yellow, whereas the cocrystals of phenoquinone are dark red. Thus, the question immediately arises whether this red color arises from the strong hydrogen-bonding interactions described above or from other, weaker, crystal packing interactions (*e.g.*, π–π interactions among the planar rings). However, no evidence for π–π stacking of aromatic rings was detected in this structure by the *OLEX2* software (Dolomanov *et al.*, 2009); thus, column–column and sheet–sheet packing forces are merely van der Waals interactions, unlikely to perturb the electronic energy levels significantly enough to cause such a drastic color change upon formation of the hydrogen-bonded complex. Moreover, as described in the *Synthesis and crys-*

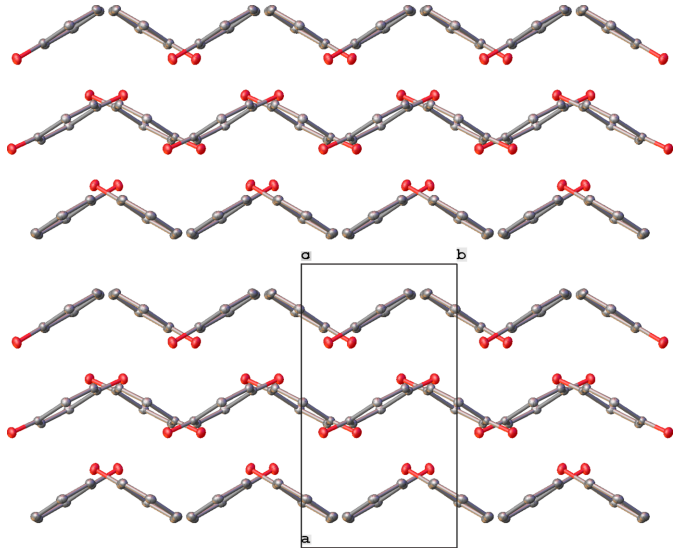

Figure 3
View along [001], showing the 62.5° angle between phenoquinone planes in adjacent sheets in the solid state (H atoms omitted for clarity).

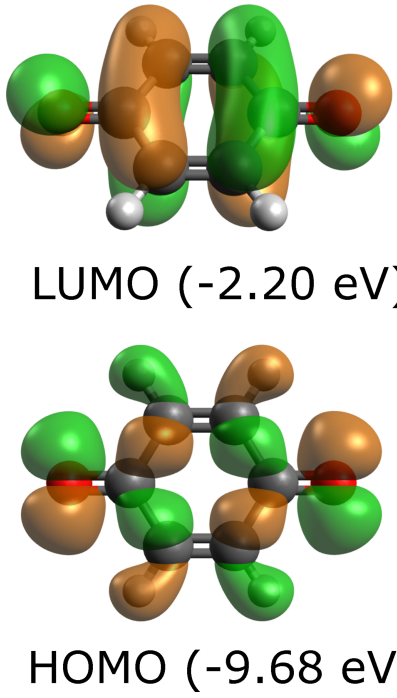

Figure 4
HOMO and LUMO molecular orbitals of *p*-benzoquinone.

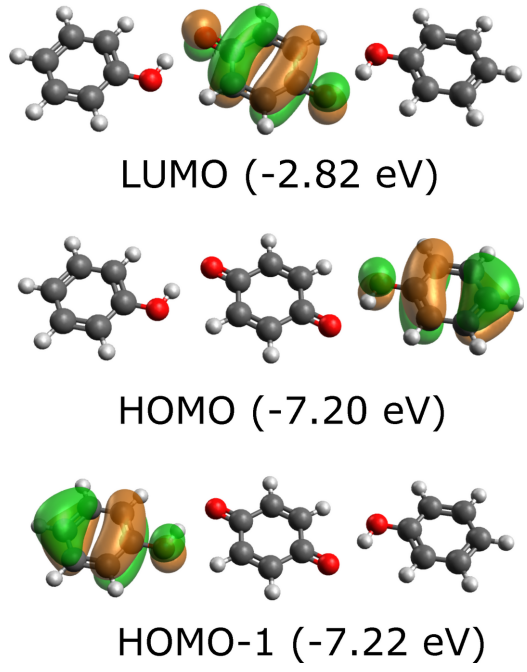

Figure 5
Near-degenerate HOMO and HOMO-1 orbitals and LUMO orbital of phenoquinone.

tallization section below, the melt that forms upon heating the two solids together is dark red. As weak van der Waals interactions are unlikely to persist in a melt at 343–344 K (Fukushima & Sakurada, 1976), the red color of solid or liquid phenoquinone was not ascribed to such interactions causing changes in electronic energy levels, but to hydrogen-bonding-induced shifts in these levels. This is unusual, because hydrogen-bonding interactions generally manifest themselves as a red-shift in vibrational frequencies, not in altered electronic states. Indeed, the *p*-benzoquinone C═O stretch shifted from 1671 cm^{-1} to 1638 cm^{-1} and the phenol O—H vibration from 3612 cm^{-1} to 3265 cm^{-1} upon hydrogen bonding (Fukushima & Sakurada, 1976). In each case, the free stretch in solution was compared to the hydrogen-bonded stretch in the solid state.

Time-dependent density functional theory (TD-DFT) calculations on phenoquinone reveal a (vibrationally coupled) charge transfer excitation responsible for its color. This type of behavior has been observed in the very similar quinhydrone (Rury *et al.*, 2017). The first excited state for *p*-benzoquinone gives rise to a HOMO–LUMO transition at 436 nm, accounting for its yellow color; the HOMO and LUMO of *p*-benzoquinone are shown in Fig. 4. Meanwhile, the two lowest excitations for phenoquinone occur at 530 and 535 nm and correspond to the HOMO-1 to LUMO and HOMO to LUMO transitions, respectively. This accounts for its red color. We note that the HOMO-1 and HOMO of phenoquinone are quasidegenerate π-antibonding orbitals predominantly on each of the phenols, with an energy difference of only 0.016 eV. The HOMO, HOMO-1 and LUMO orbitals of phenoquinone are shown in Fig. 5. The HOMO and HOMO-1 orbital are not exactly degenerate because the DFT geometry optimization of phenoquinone was carried out without any symmetry constraints, resulting in a slightly lower symmetry energy minimum. In the optimized structure, the two O—H bonds differ slightly in length (0.97247 *vs* 0.97264 Å, within the margin of error of the X-ray measurement); this difference is sufficient to lift the degeneracy of the orbital energies in the DFT calculation.

Compared to the intramolecular HOMO–LUMO transition in *p*-benzoquinone, the HOMO–LUMO transition in phenoquinone is an intermolecular charge-transfer band from much higher energy HOMO levels on the phenols, to the same LUMO predominantly on *p*-benzoquinone that now has a slightly lower energy due to the cooperative effect of the two hydrogen-bonded phenols. The upshot is that the HOMO-LUMO bandgap is significantly higher in *p*-benzoquinone (yellow) than in phenoquinone (red), accounting for the color change that occurs upon formation of the hydrogen-bonded complex.

4. Database survey

The structure of the phenoquinone cocrystal was first determined at room temperature (Sakurai, 1968) and deposited in the CSD more than 50 years ago as refcode PHENQU (CCDC No. 1232408). Prior to that, Wallwork and Harding had studied this cocrystal (Wallwork & Harding, 1953; Harding & Wallwork, 1953), but no crystal structure from their work was deposited in the CSD. Additionally, the quality of the previously obtained structural information was relatively poor because of the primitive nature of diffraction equipment at the

time, warranting a re-examination with modern diffraction methods at low temperature.

5. Synthesis and crystallization

Both phenol and *p*-benzoquinone were obtained from Acros Organics. Phenol was used as received, but *p*-benzoquinone was recrystallized by sublimation in air at 313 K before use. To a nitrogen-filled test tube sealed with a septum were added 0.109 g of *p*-benzoquinone (1 mmol) and 0.188 g of phenol (2 mmol). Upon gentle heating with a heat gun, the two solids melted together, forming a clear red liquid. The test tube containing the liquid was placed in a 313 K sand bath to cool, producing a solid mass of red laths and needles of phenoquinone several mm long within 10 minutes. The crystals thus produced were of X-ray quality. No trace of yellow *p*-benzoquinone or colorless phenol crystals were observed in the bulk, indicating complete conversion of these starting materials to red phenoquinone. See the *Supporting Information* for photomicrographs of the single crystal used for structure determination and of a bulk sample of phenoquinone.

6. Density functional theory calculations

The singlet ground-state structures for 1,4-benzoquinone and the phenoquinone complex were optimized at the M06-2X/ma-def2-SVP level of theory and basis set (Zhao & Truhlar, 2008; Zheng *et al.*, 2011). Dispersion interactions were accounted for using Grimme's D3 dispersion correction with zero damping (Grimme *et al.*, 2011). Both def2/J and def2-SVP/C auxiliary basis sets were used in the RIJCOSX approximation to speed up the calculation (Neese *et al.*, 2009). From the optimized geometries, vertical excitation energies were computed using time-dependent density functional theory (TD-DFT) within the Tamm–Dancoff approximation (TDA; Hirata & Head-Gordon, 1999) at the mPW2PLYP/ma-def2-TZVP level of theory and basis set, employing def2/J and def2-TZVP/C auxiliary basis sets. All electronic structure calculations were performed using the *ORCA 6.0* suite of programs (Neese, 2022).

7. Refinement

Crystal data, data collection and structure refinement details are summarized in Table 1. The O-bound H atom was freely refined. C-bound H atoms were positioned geometrically (C—H = 0.95 Å) and refined as riding with U_{iso}(H) = 1.2U_{eq}(C).

Acknowledgements

ATR thanks UWF for internal research funding.

Funding information

Funding for this research was provided by: National Science Foundation (grant No. DUE-0942850 to Dean H. Johnston).

Table 1
Experimental details.

Crystal data	
Chemical formula	$C_6H_4O_2{\cdot}2C_6H_6O$
M_r	296.31
Crystal system, space group	Monoclinic, $P2_1/c$
Temperature (K)	100
a, b, c (Å)	10.924 (4), 5.905 (2), 11.429 (4)
β (°)	100.203 (7)
V (Å^3)	725.5 (5)
Z	2
Radiation type	Mo $K\alpha$
μ (mm^{-1})	0.10
Crystal size (mm)	0.47 × 0.28 × 0.14
Data collection	
Diffractometer	Bruker *APEX*
Absorption correction	Multi-scan (*SADABS*; Krause *et al.*, 2015)
T_{min}, T_{max}	0.678, 0.746
No. of measured, independent and observed [$I > 2\sigma(I)$] reflections	8910, 2218, 1505
R_{int}	0.053
(sin $\theta/\lambda)_{max}$ (Å^{-1})	0.714
Refinement	
$R[F^2 > 2\sigma(F^2)]$, $wR(F^2)$, S	0.048, 0.130, 1.04
No. of reflections	2218
No. of parameters	104
H-atom treatment	H atoms treated by a mixture of independent and constrained refinement
$\Delta\rho_{max}$, $\Delta\rho_{min}$ (e Å^{-3})	0.39, −0.31

Computer programs: *APEX2* and *SAINT* V8.40B (Bruker, 2016), *SHELXT2018/2* (Sheldrick, 2015*a*), *SHELXL2019/3* (Sheldrick, 2015*b*) abnd *OLEX2* 1.5 (Dolomanov *et al.*, 2009).

References

Braga, D., Maini, L. & Grepioni, F. (2013). *Chem. Soc. Rev.* **42**, 7638–7648.
Bruker (2016). *APEX2* and *SAINT*. Bruker AXS Inc., Madison, Wisconsin, USA.
Chettri, A., Subba, A., Singh, G. P. & Bag, P. P. (2024). *J. Pharm. Pharmacol.* **76**, 1–12.
Dolomanov, O. V., Bourhis, L. J., Gildea, R. J., Howard, J. A. K. & Puschmann, H. (2009). *J. Appl. Cryst.* **42**, 339–341.
Duarte, Í., Andrade, R., Pinto, J. F. & Temtem, M. (2016). *Int. J. Pharm.* **506**, 68–78.
Fukushima, K. & Sakurada, M. (1976). *J. Phys. Chem.* **80**, 1367–1373.
Grimme, S., Ehrlich, S. & Goerigk, L. (2011). *J. Comput. Chem.* **32**, 1456–1465.
Harding, T. T. & Wallwork, S. C. (1953). *Acta Cryst.* **6**, 791–796.
Hirata, S. & Head-Gordon, M. (1999). *Chem. Phys. Lett.* **314**, 291–299.
Karimi-Jafari, M., Padrela, L., Walker, G. M. & Croker, D. M. (2018). *Cryst. Growth Des.* **18**, 6370–6387.
Krause, L., Herbst-Irmer, R., Sheldrick, G. M. & Stalke, D. (2015). *J. Appl. Cryst.* **48**, 3–10.
Narala, S., Nyavanandi, D., Srinivasan, P., Mandati, P., Bandari, S. & Repka, M. (2021). *J. Drug. Deliv. Sci. Technol.* **61**, 102209.
Neese, F. (2022). *WIREs Comput. Mol. Sci.* **12**, e1606.
Neese, F., Wennmohs, F., Hansen, A. & Becker, U. (2009). *Chem. Phys.* **356**, 98–109.
Pratt, D. S. & Gibbs, H. D. (1913). *Philipp. J. Sci., Sect. A* **8**, 51–57.
Qi, L., Li, C., Cheng, X., Hao, H. & Xie, C. (2024). *Cryst. Growth Des.* **24**, 6196–6203.
Rury, A. S., Sorenson, S. A. & Dawlaty, J. M. (2017). *J. Phys. Chem. Lett.* **8**, 181–187.
Sakurai, T. (1968). *Acta Cryst.* B**24**, 403–412.

Sheldrick, G. M. (2015*a*). *Acta Cryst.* A**71**, 3–8.
Sheldrick, G. M. (2015*b*). *Acta Cryst.* C**71**, 3–8.
Tronov, B. V. & Sokolovich, V. B. (1956). *Izvest. Tomsk. Politekh. Inst.* **83**, 91–97.
Vishweshwar, P., McMahon, J. A., Bis, J. A. & Zaworotko, M. J. (2006). *J. Pharm. Sci.* **95**, 499–516.
Wallwork, S. C. & Harding, T. T. (1953). *Nature* **171**, 40–41.
Yadav, A. V., Shete, A. S., Dabke, A. P., Kulkarni, P. V. & Sakhare, S. S. (2009). *Indian J. Pharm. Sci.* **71**, 359–370.
Zhao, Y. & Truhlar, D. G. (2008). *Theor. Chem. Acc.* **120**, 215–241.
Zheng, J., Xu, X. & Truhlar, D. G. (2011). *Theor. Chem. Acc.* **128**, 295–305.
Zuev, V. E. (1956). *Trudy Sibir. Fiz.-Tekh. Inst., Tomsk. Univ. im. V. V. Kuibysheva* **35**, 246–248.

supporting information

Acta Cryst. (2026). E**82** [https://doi.org/10.1107/S2056989026005414]

Solvent-free synthesis and low-temperature crystal structure of phenoquinone (the 1:2 *p*-benzoquinone–phenol complex)

A. Timothy Royappa, Jake A. Tan and Dean H. Johnston

Computing details

Cyclohexa-2,5-diene-1,4-dione; phenol; phenol

Crystal data

$C_6H_4O_2 \cdot 2C_6H_6O$
$M_r = 296.31$
Monoclinic, $P2_1/c$
$a = 10.924$ (4) Å
$b = 5.905$ (2) Å
$c = 11.429$ (4) Å
$\beta = 100.203$ (7)°
$V = 725.5$ (5) Å^3
$Z = 2$
$F(000) = 312$
$D_x = 1.356$ Mg m^{-3}
Mo $K\alpha$ radiation, $\lambda = 0.71073$ Å
Cell parameters from 1314 reflections
$\theta = 3.6$–29.9°
$\mu = 0.10$ mm^{-1}
$T = 100$ K
Needle, clear dark red
0.47 × 0.28 × 0.14 mm

Data collection

Bruker APEX diffractometer
Radiation source: sealed tube
Graphite monochromator
Detector resolution: 8 pixels mm^{-1}
ω and φ scans
Absorption correction: multi-scan (SADABS; Krause *et al.*, 2015)
$T_{min} = 0.678$, $T_{max} = 0.746$
8910 measured reflections
2218 independent reflections
1505 reflections with $I > 2\sigma(I)$
$R_{int} = 0.053$
$\theta_{max} = 30.5°$, $\theta_{min} = 1.9°$
$h = -15 \rightarrow 15$
$k = -8 \rightarrow 8$
$l = -16 \rightarrow 14$

Refinement

Refinement on F^2
Least-squares matrix: full
$R[F^2 > 2\sigma(F^2)] = 0.048$
$wR(F^2) = 0.130$
$S = 1.04$
2218 reflections
104 parameters
0 restraints
Primary atom site location: dual
Hydrogen site location: mixed
H atoms treated by a mixture of independent and constrained refinement
$w = 1/[\sigma^2(F_o^2) + (0.055P)^2 + 0.155P]$ where $P = (F_o^2 + 2F_c^2)/3$
$(\Delta/\sigma)_{max} < 0.001$
$\Delta\rho_{max} = 0.39$ e Å^{-3}
$\Delta\rho_{min} = -0.31$ e Å^{-3}

Special details

Geometry. All esds (except the esd in the dihedral angle between two l.s. planes) are estimated using the full covariance matrix. The cell esds are taken into account individually in the estimation of esds in distances, angles and torsion angles; correlations between esds in cell parameters are only used when they are defined by crystal symmetry. An approximate (isotropic) treatment of cell esds is used for estimating esds involving l.s. planes.

Fractional atomic coordinates and isotropic or equivalent isotropic displacement parameters (Å²)

	x	*y*	*z*	U_{iso}*/U_{eq}
O1	0.72283 (10)	0.67446 (16)	0.52280 (9)	0.0179 (2)
O2	0.59468 (9)	0.35765 (15)	0.62685 (8)	0.0171 (2)
C7	0.55232 (12)	0.1912 (2)	0.56813 (11)	0.0127 (3)
C1	0.77840 (13)	0.8436 (2)	0.59478 (12)	0.0141 (3)
C8	0.48755 (12)	0.0104 (2)	0.62234 (11)	0.0136 (3)
H8	0.481206	0.020546	0.704008	0.016*
C6	0.77270 (12)	0.8548 (2)	0.71600 (11)	0.0146 (3)
H6	0.730611	0.740504	0.751912	0.018*
C9	0.43756 (12)	−0.1677 (2)	0.55862 (11)	0.0133 (3)
H9	0.395068	−0.280318	0.595305	0.016*
C2	0.84129 (13)	1.0113 (2)	0.54273 (12)	0.0154 (3)
H2	0.845732	1.003324	0.460568	0.019*
C5	0.82913 (13)	1.0347 (2)	0.78352 (12)	0.0165 (3)
H5	0.825310	1.042669	0.865823	0.020*
C3	0.89727 (13)	1.1896 (2)	0.61127 (13)	0.0173 (3)
H3	0.940093	1.303372	0.575684	0.021*
C4	0.89117 (13)	1.2033 (2)	0.73188 (13)	0.0181 (3)
H4	0.928956	1.326279	0.778371	0.022*
H1	0.684 (2)	0.576 (4)	0.5633 (18)	0.055 (6)*

Atomic displacement parameters (Å²)

	U^{11}	U^{22}	U^{33}	U^{12}	U^{13}	U^{23}
O1	0.0218 (6)	0.0144 (4)	0.0177 (5)	−0.0035 (4)	0.0041 (4)	−0.0035 (4)
O2	0.0186 (5)	0.0143 (4)	0.0182 (5)	−0.0015 (4)	0.0029 (4)	−0.0045 (4)
C7	0.0115 (6)	0.0119 (5)	0.0141 (6)	0.0013 (5)	0.0009 (5)	0.0001 (5)
C1	0.0131 (6)	0.0126 (6)	0.0158 (6)	0.0005 (5)	0.0006 (5)	−0.0004 (5)
C8	0.0147 (6)	0.0164 (6)	0.0103 (6)	0.0000 (5)	0.0039 (5)	0.0003 (4)
C6	0.0128 (6)	0.0153 (6)	0.0158 (6)	0.0004 (5)	0.0029 (5)	0.0025 (5)
C9	0.0138 (6)	0.0125 (6)	0.0138 (6)	−0.0003 (5)	0.0033 (5)	0.0023 (5)
C2	0.0146 (7)	0.0180 (6)	0.0139 (6)	0.0013 (5)	0.0031 (5)	0.0016 (5)
C5	0.0140 (7)	0.0211 (6)	0.0139 (6)	0.0023 (5)	0.0013 (5)	0.0000 (5)
C3	0.0133 (7)	0.0164 (6)	0.0223 (7)	−0.0018 (5)	0.0029 (5)	0.0034 (5)
C4	0.0149 (7)	0.0173 (6)	0.0206 (7)	−0.0005 (5)	−0.0006 (5)	−0.0022 (5)

Geometric parameters (Å, º)

O1—C1	1.3657 (15)	C6—C5	1.3910 (18)
O1—H1	0.90 (2)	C9—H9	0.9500

O2—C7	1.2329 (15)	C2—H2	0.9500
C7—C8	1.4764 (18)	C2—C3	1.3880 (19)
C7—C9^{i}	1.4787 (18)	C5—H5	0.9500
C1—C6	1.3994 (19)	C5—C4	1.393 (2)
C1—C2	1.3969 (19)	C3—H3	0.9500
C8—H8	0.9500	C3—C4	1.394 (2)
C8—C9	1.3390 (18)	C4—H4	0.9500
C6—H6	0.9500		

C1—O1—H1	111.4 (13)	C8—C9—C7^{i}	120.83 (11)
O2—C7—C8	120.63 (12)	C8—C9—H9	119.6
O2—C7—C9^{i}	121.47 (12)	C1—C2—H2	120.1
C8—C7—C9^{i}	117.88 (11)	C3—C2—C1	119.89 (12)
O1—C1—C6	122.55 (12)	C3—C2—H2	120.1
O1—C1—C2	117.49 (12)	C6—C5—H5	119.6
C2—C1—C6	119.95 (12)	C6—C5—C4	120.77 (12)
C7—C8—H8	119.4	C4—C5—H5	119.6
C9—C8—C7	121.28 (12)	C2—C3—H3	119.7
C9—C8—H8	119.4	C2—C3—C4	120.55 (13)
C1—C6—H6	120.2	C4—C3—H3	119.7
C5—C6—C1	119.51 (12)	C5—C4—C3	119.33 (13)
C5—C6—H6	120.2	C5—C4—H4	120.3
C7^{i}—C9—H9	119.6	C3—C4—H4	120.3

O1—C1—C6—C5	−178.57 (12)	C6—C1—C2—C3	−0.4 (2)
O1—C1—C2—C3	178.69 (12)	C6—C5—C4—C3	−0.5 (2)
O2—C7—C8—C9	177.81 (12)	C9^{i}—C7—C8—C9	−1.1 (2)
C7—C8—C9—C7^{i}	1.1 (2)	C2—C1—C6—C5	0.51 (19)
C1—C6—C5—C4	0.0 (2)	C2—C3—C4—C5	0.6 (2)
C1—C2—C3—C4	−0.1 (2)		

Symmetry code: (i) −*x*+1, −*y*, −*z*+1.

Hydrogen-bond geometry (Å, º)

D—H···*A*	*D*—H	H···*A*	*D*···*A*	*D*—H···*A*
O1—H1···O2	0.90 (2)	1.84 (2)	2.7318 (15)	172.3 (19)